

ETSCL: An Evidence Theory-Based Supervised Contrastive Learning Framework for Multi-modal Glaucoma Grading

Zhiyuan Yang^{1*}[0009-0007-8277-5772], Bo Zhang^{2*}[0009-0002-3736-4070], Yufei Shi³[0000-0003-1822-1621], Ningze Zhong⁴[0009-0007-6758-058X], Johnathan Loh⁵[0000-0001-8176-0498], Huihui Fang²[0000-0003-3380-7970], Yanwu Xu^{6**}[0000-0002-1779-931X], and Si Yong Yeo^{3**}[0000-0001-6403-6019]

¹ Beihang University, China

² College of Computing and Data Science, Nanyang Technological University, Singapore

³ Lee Kong Chian School of Medicine, Nanyang Technological University, Singapore

⁴ Sun Yat-sen University, China

⁵ National University of Singapore, Singapore

⁶ South China University of Technology, China

Abstract. Glaucoma is one of the leading causes of vision impairment. Digital imaging techniques, such as color fundus photography (CFP) and optical coherence tomography (OCT), provide quantitative and noninvasive methods for glaucoma diagnosis. Recently, in the field of computer-aided glaucoma diagnosis, multi-modality methods that integrate the CFP and OCT modalities have achieved greater diagnostic accuracy compared to single-modality methods. However, it remains challenging to extract reliable features due to the high similarity of medical images and the unbalanced multi-modal data distribution. Moreover, existing methods overlook the uncertainty estimation of different modalities, leading to unreliable predictions. To address these challenges, we propose a novel framework, namely ETSCL, which consists of a contrastive feature extraction stage and a decision-level fusion stage. Specifically, the supervised contrastive loss is employed to enhance the discriminative power in the feature extraction process, resulting in more effective features. In addition, we utilize the Frangi vesselness algorithm as a preprocessing step to incorporate vessel information to assist in the prediction. In the decision-level fusion stage, an evidence theory-based multi-modality classifier is employed to combine multi-source information with uncertainty estimation. Extensive experiments demonstrate that our method achieves state-of-the-art performance. The code is available at <https://github.com/master-Shix/ETSCL>.

Keywords: Glaucoma grading · Multi-modal learning · Contrastive learning · Evidence theory

* Zhiyuan Yang and Bo Zhang contributed equally.

** Yanwu Xu and Si Yong Yeo are the corresponding authors. Email: xuyanwu@scut.edu.cn, siyong.yeo@ntu.edu.sg

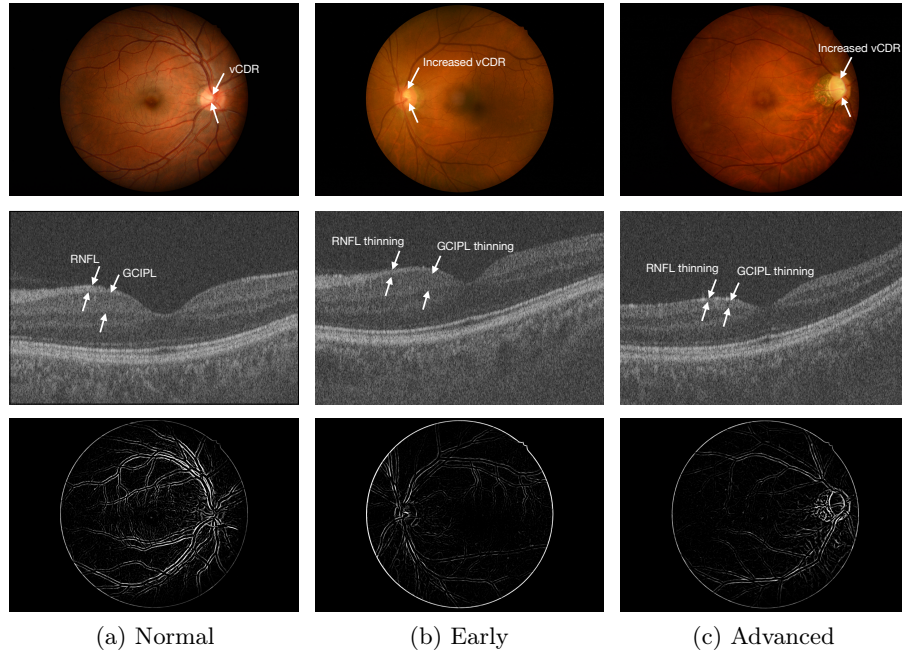


Fig. 1. Multi-modal imaging from the GAMMA dataset demonstrates glaucoma progression across three stages. Column (a) features images without glaucoma. Column (b) features early-stage glaucoma. Column (c) features intermediate-advanced-stage glaucoma. The top row displays CFP images, showing increased vCDR. The middle row displays OCT samples, showing thinning of the RNFL and GCIPL. The bottom row displays vessel structures, extracted from CFP images.

1 Introduction

Glaucoma, a leading cause of vision impairment, causes progressive damage to the optic nerve, including the optic nerve head (ONH), the retinal nerve fibre layer (RNFL) and the ganglion cell-inner plexiform layer (GCIPL) [1]. Digital imaging techniques, such as color fundus photography (CFP) [2] and optical coherence tomography (OCT) [3,4], offer quantitative and noninvasive ways to evaluate the optic nerve structure for glaucoma diagnosis. In Fig. 1 (top and middle), we showcase detailed CFP and OCT samples, demonstrating the glaucoma progression across three stages and highlighting the evolution of key clinical measures, such as the vertical Cup-to-Disc Ratio (vCDR) and the thickness of the RNFL and GCIPL.

In the field of computer-aided glaucoma diagnosis, previous studies have primarily focused on using either CFP [5,6,7] or OCT [8,9,10] individually. However, there is less exploration in multi-modality methods that utilize both modalities simultaneously. The GAMMA challenge [11], which introduces the first public multi-modality dataset, aims to advance the research in multi-modality glau-

coma grading using both CFP and OCT. MM-MIL [12] employs over-sampling to augment CFP data, aiming to balance the multi-modal data distribution. Corolla [13] introduces the extraction of the retinal thickness map as an alternative modality, leading to more efficient calculations and reduced memory usage. MM-RAF [14] develops a feature-level fusion strategy that facilitates cross-modality correlation, with an emphasis on leveraging spatial interaction between modalities through co-attention mechanism. Although existing methods [11,12,13,14] have demonstrated impressive performance, they still face several challenges: First, current methods simply concatenate feature embeddings from separate feature encoders in the final stage, overlooking the unique uncertainty estimation inherent to each modality. The approach that treats all modalities with equal weight can result in unreliable predictions. Furthermore, given the inherently high similarity of medical images and the scarcity of labeled medical datasets, standard supervised learning methods often produce sub-optimal and inconsistent feature representations.

To address the challenges discussed above, we propose a novel framework, namely ETSCCL, which consists of a contrastive feature extraction stage and a decision-level fusion stage. In the contrastive feature extraction stage, we employ the supervised contrastive loss to enhance the discriminative power, resulting in more effective feature extraction. In addition, we utilize the Frangi vesselness algorithm [15] as a preprocessing step to incorporate previously neglected vessel information as a third complementary branch alongside the CFP and OCT branches. In the decision-level fusion stage, we propose a multi-modality classifier based on the evidence theory [16,17]. The proposed classifier uses the belief functions to quantitatively estimate the uncertainty of information from different modalities, and combines the information based on Dempster’s rule of combination. To the best of our knowledge, our framework represents the first attempt of applying decision-level fusion and vessel information in the multi-modality glaucoma grading problem. Extensive experiments on the public GAMMA dataset [11] demonstrate that our method achieves state-of-the-art (SOTA) performance.

2 Methodology

As shown in Fig. 2, the framework is trained in two stages. In the contrastive feature extraction stage, alongside the CFP and OCT branches, vessel information is extracted from the CFP images as a third complementary branch. Vascular genesis is considered a key triggering factor in the development of glaucoma [18,19]. However, vessel information has been overlooked in previous glaucoma grading methods. As a preprocessing step, we employ the Frangi filter [15] to extract vessel information from the CFP images. Fig. 1 (bottom) illustrates the extracted vessel structures. Then the supervised contrastive loss is employed to train the three feature encoders separately, generating reliable feature embeddings. In the decision-level fusion stage, we develop an evidence theory-based classifier to fuse information from multiple sources, utilizing uncertainty estimation across different modalities.

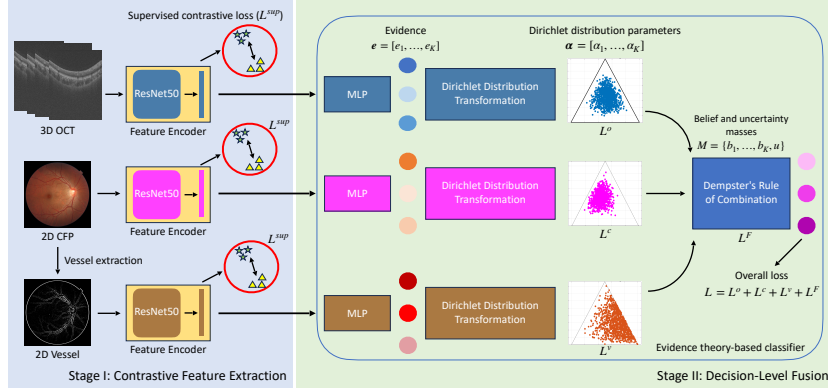


Fig. 2. Overview of the proposed ETSCl framework.

2.1 Contrastive Feature Extraction

In clinical practice, extracting glaucoma-indicative features from CFP and OCT images using traditional convolutional neural networks is challenging due to the high similarity of medical images and the unbalanced multi-modal data distribution. Compared to traditional supervised learning, contrastive learning [20,21,22,23] leverages the semantic similarity between data points to generate more stable representations for downstream tasks. This strategy has influenced the development of existing methods such as Corolla [13] and MM-RAF [14]. As inspired by the work of [22], we implement a supervised contrastive learning strategy. Given N randomly sampled pairs $\{x_h, y_h\}_{h=1}^N$, the augmented batch for contrastive learning comprises $2N$ pairs $\{\tilde{x}_h, \tilde{y}_h\}_{h=1}^{2N}$, where $y_h = \tilde{y}_{2h} = \tilde{y}_{2h-1}$. Let $i \in I = \{1, \dots, 2N\}$ be the index of an augmented sample. The *positive* is the index of the other augmented sample derived from the same sample i . The embedding vectors \mathbf{z} , with \mathbf{z}_i representing the embedding vector for sample i , are derived via the encoder and projection head. The supervised contrastive loss [22] is generalized from the self-supervised contrastive loss [20,21], and takes the form of:

$$L^{sup} = \sum_{i \in I} \frac{-1}{|P(i)|} \sum_{p \in P(i)} \log \frac{\exp(\mathbf{z}_i \cdot \mathbf{z}_p / \tau)}{\sum_{\alpha \in A(i)} \exp(\mathbf{z}_i \cdot \mathbf{z}_\alpha / \tau)}, \quad (1)$$

where the \cdot symbol denotes the inner dot product, τ is a scalar temperature parameter, $A(i) = I \setminus \{i\}$, and $P(i) = \{p \in A(i) : \tilde{y}_p = \tilde{y}_i\}$ is the set of indices of all the positives in the augmented batch. The supervised contrastive loss leverages label information to generate the positives, making it more effective at grouping features of the same class closely together and separating those of different classes.

2.2 Decision-Level Fusion

After feature extraction, the information from different modalities is integrated in the classifier. The evidence theory, also known as the Dempster-Shafer Theory (DST) [16,17], introduces the concept of *belief* to quantify the uncertainty of evidence. Informed by recent developments in DST-based multi-view classification [24,25], we design a multi-modality classifier to integrate multi-source information more effectively. In the decision-level fusion stage, the output of the multilayer perceptron (MLP) is regarded as *evidence*, denoting the support for each class. For each modality, we employ the Softplus function on the feature embeddings to obtain the evidence values of all classes. The Dirichlet distribution is adopted to produce more reliable class probabilities for each modality, with the loss function designed accordingly. Subsequently, Dempster’s rule of combination is employed to integrate multiple Dirichlet distributions from different modalities.

Dirichlet distribution Given N labeled samples $\{(x_1, y_1), \dots, (x_N, y_N)\}$, conventional classifiers employ a Softmax layer to estimate the class probabilities. Mathematically, the Softmax layer’s outputs can be interpreted as parameters for a multinomial distribution. For a sample with index i , the probabilities of K classes are $\boldsymbol{\mu}_i = [\mu_{i1}, \dots, \mu_{iK}]$. The optimization process of Maximum Likelihood Estimation (MLE), with respect to the network’s parameters θ , is defined as follows:

$$\arg \max_{\theta} \text{Mult}(\mathbf{Y}; \theta) = \prod_{i=1}^N \prod_{j=1}^K \mu_{ij}^{y_{ij}}, \quad (2)$$

where y_{ij} is an indicator that is 1 if the sample i belongs to class j and 0 otherwise. Minimizing the log-likelihood, an approach widely known as the *cross-entropy loss*, essentially mirrors the objective of MLE. Given its limitations as a frequentist technique, MLE often struggles to effectively handle varying conditions and small data scenarios, which can result in overconfidence in the estimates. Alternatively, we employ the Dirichlet distribution as the conjugate prior for the multinomial distribution, allowing for more reliable and robust statistical inference. For the sample with index i , Dirichlet distribution is defined by K parameters $\boldsymbol{\alpha}_i = [\alpha_{i1}, \dots, \alpha_{iK}]$. The probability density function of the Dirichlet distribution is:

$$\text{Dir}(\boldsymbol{\mu}_i \mid \boldsymbol{\alpha}_i) = \begin{cases} \frac{1}{B(\boldsymbol{\alpha}_i)} \prod_{j=1}^K \mu_{ij}^{\alpha_{ij}-1} & \text{for } \boldsymbol{\mu}_i \in S_{unit}^{K-1}, \\ 0 & \text{otherwise,} \end{cases} \quad (3)$$

where S_{unit}^{K-1} denotes the $K - 1$ dimensional unit simplex, and $B(\boldsymbol{\alpha}_i)$ represents the K -dimensional multivariate beta function. Consequently, label prediction for sample i is modeled as a generative process:

$$\mathbf{y}_i \sim \text{Mult}(\mathbf{y}_i \mid \boldsymbol{\mu}_i), \quad \boldsymbol{\mu}_i \sim \text{Dir}(\boldsymbol{\mu}_i \mid \boldsymbol{\alpha}_i). \quad (4)$$

To design the loss function for the Dirichlet distribution of a single sample with index i and label \mathbf{y}_i , given the Dirichlet distribution parameters $\boldsymbol{\alpha}_i$, the Mean Square Error (MSE) loss is derived as follows:

$$\begin{aligned} \text{MSE}_i &= \int_{\boldsymbol{\mu}_i \in S_{unit}^{K-1}} \|\mathbf{y}_i - \boldsymbol{\mu}_i\|_2^2 \cdot \text{Dir}(\boldsymbol{\mu}_i \mid \boldsymbol{\alpha}_i) d\boldsymbol{\mu}_i = \mathbb{E} \left[\sum_{j=1}^K (y_{ij} - \mu_{ij})^2 \right] \\ &= \sum_{j=1}^K (y_{ij}^2 - 2y_{ij}\mathbb{E}[\mu_{ij}] + \mathbb{E}[\mu_{ij}^2]) = \sum_{j=1}^K (y_{ij} - \mathbb{E}[\mu_{ij}])^2 + \text{Var}(\mu_{ij}) \\ &= \sum_{j=1}^K \left(y_{ij} - \frac{\alpha_{ij}}{S_i} \right)^2 + \frac{\alpha_{ij}(S_i - \alpha_{ij})}{S_i^2(S_i + 1)}, \end{aligned} \quad (5)$$

where $S_i = \sum_{j=1}^K \alpha_{ij}$, known as the Dirichlet strength. To counteract any drift towards an unrealistic distribution, a penalty term derived from the Kullback-Leibler (KL) divergence, is incorporated to adjust the Dirichlet distribution of the sample i accordingly. Consequently, the loss function for this Dirichlet distribution is:

$$L_i = \text{MSE}_i + \lambda_i \cdot \text{KL}[\text{Dir}(\boldsymbol{\mu}_i \mid \boldsymbol{\alpha}_i) \parallel \text{Dir}(\boldsymbol{\mu}_i \mid \mathbf{1})], \quad (6)$$

where $\mathbf{1}$ represents a K -dimensional unit vector, and λ_i is the annealing coefficient.

Belief, uncertainty and combination Subjective logic (SL) [26] provides a framework that links the Dirichlet distribution parameters to the belief and uncertainty associated with each class. For the Dirichlet distribution of a single sample, SL assigns a belief mass b_j to class j , reflecting the confidence in the occurrence of each class. An aggregate uncertainty mass u quantifies the overall uncertainty across all classes. The summation of belief masses of all classes and the uncertainty mass equals 1, ensuring a normalized representation of belief and uncertainty. Given the evidence e_j for class j , the Dirichlet distribution parameter, α_j , is calculated as $\alpha_j = e_j + 1$. The belief masses \mathbf{b} and the uncertainty mass u are derived from the Dirichlet distribution parameters as follows:

$$\mathbf{b} = \frac{\mathbf{e}}{S} = \frac{\boldsymbol{\alpha} - \mathbf{1}}{S}, \quad u = \frac{K}{S}, \quad (7)$$

where $\boldsymbol{\alpha} - \mathbf{1}$ indicates the subtraction of 1 from each parameter in the Dirichlet distribution parameter vector $\boldsymbol{\alpha}$, and $S = \sum_{j=1}^K (e_j + 1) = \sum_{j=1}^K \alpha_j$, known as the Dirichlet strength. We then adopt a reduced Dempster's combination rule [24] to manage computational complexity by avoiding the large numbers of input and output masses in the original rule. For the fusion of the CFP and OCT branches, the mass set of the fusion $M^F = \{b_1^F, \dots, b_K^F, u^F\}$ is calculated from the mass sets of the CFP branch $M^c = \{b_1^c, \dots, b_K^c, u^c\}$ and the OCT branch

$M^o = \{b_1^o, \dots, b_K^o, u^o\}$ as follows:

$$b_j^F = \frac{1}{1 - K'}(b_j^c b_j^o + b_j^c u^o + b_j^o u^c), u^F = \frac{1}{1 - K'} u^c u^o, \quad (8)$$

where $K' = \sum_{j \neq i} b_j^c b_i^o$ is the conflict measure between the CFP and OCT branches. Then we apply the same computation to combine this CFP and OCT fusion M^F with the Vessel branch to calculate the final mass set. Subsequently, based on the final mass set, we can obtain the corresponding parameters of the joint Dirichlet distribution.

Evidence theory-based classifier After deriving the joint Dirichlet distribution from different modalities, the class with the highest probability is identified as the final prediction output. Based on Eq. (6), the loss for each modality is calculated as the summation of losses for all samples: $\sum_{i=1}^N L_i$. Consequently, we have the losses for the CFP, OCT, and Vessel branches, denoted as L^c , L^o , and L^v , respectively. Additionally, we sum up the loss of the joint Dirichlet distribution across all samples to calculate the fusion loss, L^F . The overall loss function of the classifier is then calculated as the summation of the losses from all the modalities and the fusion loss, as illustrated in Fig. 2.

3 Experiments

3.1 Dataset

The public GAMMA dataset [11] consists of 300 pairs of CFP images and OCT volumes, with each OCT volume consisting of 256 2D slices. The dataset is categorized into three labels: non-glaucoma, early-glaucoma, and intermediate-advanced-glaucoma, presenting a multiclass classification task. We divide the dataset into 200 samples for training and 100 samples for testing.

3.2 Implementation Details

All experiments are conducted on two NVIDIA A40 GPUs. For image augmentation, we apply normalization, color jittering, random grayscale conversion, center cropping, and random horizontal flipping. In the feature extraction stage, we utilize ResNet50, pretrained on ImageNet, as the backbone for all the three branches. We process the 3D OCT inputs as 256-channel 2D images. For each feature encoder, we then employ 2 fully-connected layers with ReLU activation to generate a 128-dimensional tensor, which is subsequently used for the supervised contrastive loss L^{sup} , with the temperature parameter τ set to 0.05. The network is trained using Adam optimizer, with a learning rate of 0.001 and a batch size of 14, over 10 epochs. In the decision-level fusion stage, the embeddings generated by each feature encoder from the previous stage are independently passed to separate MLP networks. Each MLP, with an input size of 128 and an output size of 3, is trained using the Adam optimizer over 200 epochs.

Table 1. Performance of the baselines and our ETSCCL on the GAMMA dataset.

Method		Kappa	Accuracy
Single-modality	CFP - ResNet	0.6199	0.68
	OCT - ResNet	0.5006	0.62
	OCT - 3D EfficientNet	0.4930	0.60
Multi-modality	CFP+OCT - Dual ResNet	0.7129	0.75
	CFP+OCT - ResNet+3D EfficientNet	0.7200	0.75
	GAMMA challenge winner [11]	0.8535	0.81
	ETSCCL	0.8844	0.84

Table 2. Ablation study results on the GAMMA dataset. CFP means the presence of the CFP branch. OCT means the presence of the OCT branch. Vessel denotes the addition of the Vessel branch. SCL indicates the use of the supervised contrastive loss. ET represents the evidence theory-based classifier.

CFP	OCT	Vessel	SCL	ET	Kappa	Accuracy
✓					0.6199	0.68
✓	✓				0.7129	0.75
✓	✓	✓			0.7478	0.77
✓			✓		0.8170	0.77
✓	✓		✓		0.8273	0.80
✓	✓	✓	✓		0.8592	0.81
✓	✓	✓	✓	✓	0.8844	0.84

3.3 Results and Ablation Study

Following the evaluation approach in the GAMMA challenge, we use Cohen’s kappa coefficient as the primary metric and accuracy as the secondary metric. For this ordinal ternary classification task, kappa is quadratically weighted to reflect the varying degrees of disagreement across ordinal categories [11], which is particularly effective in assessing models on unbalanced datasets.

We select both single-modality and multi-modality methods as the baselines. For the single-modality baselines, ResNet50 is selected for CFP, while ResNet50 and 3D EfficientNet are selected for OCT. For the multi-modality baselines, we choose a dual-branch ResNet50, and a hybrid of ResNet50 for CFP and 3D EfficientNet for OCT. Additionally, the GAMMA challenge winner’s method is selected as another multi-modality baseline. As shown in Table 1, our method outperforms the best baseline, the GAMMA challenge winner, by over 3% in kappa and by 3% in accuracy.

As shown in Table 2, the improvements observed when adding the supervised contrastive loss to conventional CFP, dual branches (CFP and OCT), and triple branches (CFP, OCT, and Vessel) demonstrate the significant contribution of the supervised contrastive loss. Furthermore, comparisons between dual branches (CFP and OCT) and triple branches (CFP, OCT, and Vessel), both with and without the supervised contrastive loss, validate the benefit of incorporating the vessel information. Lastly, the advancement from using the conventional Softmax layer to using the evidence theory-based classifier in the triple branches (CFP,

Table 3. Comparison between our ETSCL and other SOTA methods on the GAMMA dataset. † Corolla uses 100 samples for training and testing. * MM-RAF trains on a private dataset and tests with 100 GAMMA samples on both its method and MM-MIL.

Method	Kappa
Corolla† [13]	0.8550
MM-MIL* [12]	0.8562
MM-RAF* [14]	0.8467
ETSCL	0.8844

OCT, and Vessel) highlights the superior performance of the evidence theory-based classifier.

In Table 3, we present a comparison of our ETSCL with other SOTA methods that were published after the GAMMA challenge. We include only the kappa values as reported in their respective publications, since not all studies disclose their accuracy. Among these published SOTA methods, our ETSCL achieves the highest kappa. It is worth noting that this comparison might not be strict, due to variations in the datasets used by each method.

4 Conclusion

In this study, we propose an evidence theory-based supervised contrastive learning framework for multi-modality glaucoma grading. The supervised contrastive loss is employed to extract effective feature embeddings. To integrate multi-modality information with uncertainty estimation, we design an evidence theory-based classifier. In addition, vessel information is utilized to assist in the prediction. However, the limited size of the GAMMA dataset constrains our method choices, such as Vision Transformer which often leads to overfitting. The lack of private datasets restricts our ability to further test the generalizability and robustness of our method, as the GAMMA dataset is currently the only high-quality public dataset with multi-stage glaucoma grading. Furthermore, subsequent generalizability tests can reinforce the validation of the Vessel branch’s efficacy, considering the novelty of incorporating vessel information.

Acknowledgments. This project is supported by the Ministry of Education, Singapore, under its Academic Research Fund Tier 1 (RS16/23).

Disclosure of Interests. The authors have no competing interests to declare that are relevant to the content of this article.

References

1. Weinreb, R.N., Leung, C.K., Crowston, J.G., Medeiros, F.A., Friedman, D.S., Wiggs, J.L., Martin, K.R.: Primary open-angle glaucoma. *Nature Reviews Disease Primers* **2**(1), 1–19 (2016)

2. Besenczi, R., Tóth, J., Hajdu, A.: A review on automatic analysis techniques for color fundus photographs. *Computational and Structural Biotechnology Journal* **14**, 371–384 (2016)
3. Huang, D., Swanson, E.A., Lin, C.P., Schuman, J.S., Stinson, W.G., Chang, W., Hee, M.R., Flotte, T., Gregory, K., Puliafito, C.A., et al.: Optical coherence tomography. *Science* **254**(5035), 1178–1181 (1991)
4. De Fauw, J., Ledsam, J.R., Romera-Paredes, B., Nikolov, S., Tomasev, N., Blackwell, S., Askham, H., Glorot, X., O’Donoghue, B., Visentin, D., et al.: Clinically applicable deep learning for diagnosis and referral in retinal disease. *Nature Medicine* **24**(9), 1342–1350 (2018)
5. Al-Bander, B., Al-Nuaimy, W., Al-Taei, M.A., Zheng, Y.: Automated glaucoma diagnosis using deep learning approach. In: *Proceedings of the 14th International Multi-Conference on Systems, Signals & Devices (SSD)*. pp. 207–210 (2017)
6. Fang, H., Li, F., Wu, J., Fu, H., Sun, X., Son, J., Yu, S., Zhang, M., Yuan, C., Bian, C., et al.: Refuge2 challenge: A treasure trove for multi-dimension analysis and evaluation in glaucoma screening. *arXiv preprint arXiv:2202.08994* (2022)
7. He, H., Lin, L., Cai, Z., Tang, X.: Joined: Prior guided multi-task learning for joint optic disc/cup segmentation and fovea detection. In: *Proceedings of the International Conference on Medical Imaging with Deep Learning (MIDL)*. pp. 477–492 (2022)
8. Asaoka, R., Hirasawa, K., Iwase, A., Fujino, Y., Murata, H., Shoji, N., Araie, M.: Validating the usefulness of the “random forests” classifier to diagnose early glaucoma with optical coherence tomography. *American Journal of Ophthalmology* **174**, 95–103 (2017)
9. Maetschke, S., Antony, B., Ishikawa, H., Wollstein, G., Schuman, J., Garnavi, R.: A feature agnostic approach for glaucoma detection in oct volumes. *PLoS One* **14**(7), e0219126 (2019)
10. Wang, H., Guo, X., Song, K., Sun, M., Shao, Y., Xue, S., Zhang, H., Zhang, T.: Oct-former: An efficient hierarchical transformer network specialized for retinal optical coherence tomography image recognition. *IEEE Transactions on Instrumentation and Measurement* **72**, 1–17 (2023)
11. Wu, J., Fang, H., Li, F., Fu, H., Lin, F., Li, J., Huang, Y., Yu, Q., Song, S., Xu, X., et al.: Gamma challenge: glaucoma grading from multi-modality images. *Medical Image Analysis* **90**, 102938 (2023)
12. Li, X., Zhou, Y., Wang, J., Lin, H., Zhao, J., Ding, D., Yu, W., Chen, Y.: Multi-modal multi-instance learning for retinal disease recognition. In: *Proceedings of the 29th ACM International Conference on Multimedia*. pp. 2474–2482 (2021)
13. Cai, Z., Lin, L., He, H., Tang, X.: Corolla: An efficient multi-modality fusion framework with supervised contrastive learning for glaucoma grading. In: *Proceedings of the 19th International Symposium on Biomedical Imaging (ISBI)*. pp. 1–4 (2022)
14. Zhou, Y., Yang, G., Zhou, Y., Ding, D., Zhao, J.: Representation, alignment, fusion: A generic transformer-based framework for multi-modal glaucoma recognition. In: *Proceedings of the 26th International Conference on Medical Image Computing and Computer-Assisted Intervention (MICCAI)*. pp. 704–713 (2023)
15. Frangi, A.F., Niessen, W.J., Vincken, K.L., Viergever, M.A.: Multiscale vessel enhancement filtering. In: *Proceedings of the First International Conference on Medical Image Computing and Computer-Assisted Intervention (MICCAI)*. pp. 130–137 (1998)
16. Shafer, G.: *A Mathematical Theory of Evidence*, vol. 42. Princeton University Press, Princeton, NJ (1976)

17. Dempster, A.P.: Upper and lower probabilities induced by a multivalued mapping. In: *Classic Works of the Dempster-Shafer Theory of Belief Functions*, vol. 219, pp. 57–72. Springer Berlin Heidelberg, Berlin, Heidelberg (2008)
18. Cherecheanu, A.P., Garhofer, G., Schmidl, D., Werkmeister, R., Schmetterer, L.: Ocular perfusion pressure and ocular blood flow in glaucoma. *Current Opinion in Pharmacology* **13**(1), 36–42 (2013)
19. Wang, L., Cull, G.A., Fortune, B.: Optic nerve head blood flow response to reduced ocular perfusion pressure by alteration of either the blood pressure or intraocular pressure. *Current Eye Research* **40**(4), 359–367 (2015)
20. Chen, T., Kornblith, S., Norouzi, M., Hinton, G.: A simple framework for contrastive learning of visual representations. In: *Proceedings of the 37th International Conference on Machine Learning*. pp. 1597–1607 (2020)
21. Henaff, O.: Data-efficient image recognition with contrastive predictive coding. In: *Proceedings of the 37th International Conference on Machine Learning*. pp. 4182–4192 (2020)
22. Khosla, P., Teterwak, P., Wang, C., Sarna, A., Tian, Y., Isola, P., Maschinot, A., Liu, C., Krishnan, D.: Supervised contrastive learning. *Advances in Neural Information Processing Systems* **33**, 18661–18673 (2020)
23. Chen, X., Xie, S., He, K.: An empirical study of training self-supervised vision transformers. In: *Proceedings of the IEEE/CVF International Conference on Computer Vision*. pp. 9640–9649 (2021)
24. Han, Z., Zhang, C., Fu, H., Zhou, J.T.: Trusted multi-view classification with dynamic evidential fusion. *IEEE Transactions on Pattern Analysis and Machine Intelligence* **45**(2), 2551–2566 (2023)
25. Liu, W., Chen, Y., Yue, X., Zhang, C., Xie, S.: Safe multi-view deep classification. In: *Proceedings of the AAAI Conference on Artificial Intelligence*. vol. 37, pp. 8870–8878 (2023)
26. Jøsang, A.: *Subjective Logic: A Formalism for Reasoning Under Uncertainty*. Springer Cham (2016)